Anal. Chem. **2006,** *78,* 5685−5692

Capillary Electrophoresis Absorption Detection Using Fiber-Loop Ring-Down Spectroscopy

Runkai Li, Hans-Peter Loock,* and Richard D. Oleschuk*

Department of Chemistry, Queen's University, Kingston, Ontario, Canada, K7L 3N6

The application of phase-shift, fiber-loop, ring-down spectroscopy (PS-FLRDS) as an on-line detector for capillary electrophoresis (CE) of biomolecules is demonstrated. CE was conducted using a custom-designed capillary/fiber interface coupled to an absorption detector, which is based on the ring-down of an optical signal in a closed fiber waveguide loop. The ring-down times were obtained by measuring the phase difference between intensity modulated light entering and exiting the fiber loop. The incorporation of a microlens to enhance transmission through the sample gap led to an improvement of the sensitivity by up to 80% compared to the square-cut fiber and a reduction in the detection limit. The performance of the PS-FLRDS absorption technique as an online detector was characterized by flow injection through a capillary. Good repeatability and linear response were obtained, and the detection limit using the lensed fiber/capillary interface system was determined to be $\alpha_{min} = 1.6\ cm^{-1}$ for an absorption path of ~30 μm. PS-FLRDS coupled to CE was also applied to the analysis of human serum albumin (HSA) by using a NIR dye as a noncovalent label. The excess free dye and the dye/protein complex were resolved. The labeling coefficient was determined to be ~6, and good repeatability of peak areas (RSD = 8.7%) was obtained for the analysis of HSA. Furthermore, an excellent linear response ($R^2 > 0.99$) was obtained between the peak areas and concentrations of HSA. The detection limit of labeled HSA was determined to be 1.67 μM.

Capillary electrophoresis (CE) has become a popular analytical method for separation and analysis of complex mixtures, such as environmental, biological, and medicinal samples, mainly because of the high separation resolution it offers. Many methods of detection have been combined with capillary electrophoresis, with fluorescence detection and UV−visible absorption being the most frequently used. For label-free detection, UV−visible absorption has been the most common as a result of its universality and sensitivity (10^{-5}−10^{-6} M[1]). UV−visible detection would likely be more widespread, were it not limited in sensitivity. Capillaries used for CE typically have an inner diameter of ~100 μm, resulting in poor sensitivity for analytes with low molar extinction coefficients due to the short absorption path lengths.[2−5] To improve the absorption detection limits of UV−visible detectors, several attempts have been made to increase the path length, for example, by changing the shape or diameter of the capillary in the detection area. Here, "Z",[6−8] "U", or bubble[9,10] cells have been very effective and were shown to increase signal-to-noise (S/N) ratios by up to 20 and 60 times, respectively, compared to the single-pass UV−visible absorption detection. However, extending the path length in a single-pass cell is directly correlated with a loss of temporal resolution. Multireflection nanoliter-scale cells offer a conceptually superior solution.[11] On the other hand, the necessity to maintain accurate alignment of the absorption path may restrict not so much the sensitivity and time resolution but the stability and robustness of the cell. Furthermore, all traditional absorption techniques suffer from problems associated with measuring small intensity changes in the presence of a relatively large intensity background.[12] In addition, lasers as intense light sources often exhibit intensity fluctuations with time and laser wavelength, which limits their usefulness in absorbance applications. Therefore, the lack of sensitivity and robustness is still considered the fundamental limitation of UV−visible detection techniques in CE applications.

A similar problem in gas-phase absorption spectroscopy has been elegantly solved by cavity ring-down spectroscopy (CRDS),[13−17] a technique that is largely insensitive to light intensity fluctuations, since the optical loss (absorption) is inferred from the rate of the intensity change. By measuring the build-up and ring-down of light

* To whom correspondence should be addressed. E-mail: oleschuk@chem.queensu.ca; hploock@chem.queensu.ca.

(1) Landers, J. P., Ed. *Handbook of Capillary Electrophoresis,* 2nd ed.; CRC Press: Boca Raton, FL, 1997.
(2) Grant, I. H.; Steuer, W. *J. Microcolumn Sep.* **1990**, *2*, 74−80.
(3) Tsudea, T.; Sweedler, J, V.; Zare, R. N. *Anal. Chem.* **1990**, *62*, 2149−2152.
(4) Taylor, J. A.; Yeung, E. S. *J. Chromatogr.* **1991**, *550*, 831−837.
(5) Poppe, H. *Anal. Chim. Acta* **1980**, *114*, 59−70.
(6) Chervet, J. P.; Van Soest, R. E. J.; Ursem, M. *LC Packings*, Technical Communication, San Francisco, CA, 1990.
(7) Wang, T.; Aiken, J. H.; Huie, C. W.; Hartwick, R. A. *Anal. Chem.* **1991**, *63*, 1372−1376.
(8) Kaltenbach, P.; Ross, G.; Heiger, D. N. *HPCE 1997*, Anaheim, CA, 1997.
(9) Lin, Y. W.; Huang, C. C.; Chang, H. T. *Anal. Bioanal. Chem.* **2003**, *376* (3), 379−383.
(10) Tseng, W. L.; Lin Yang, W.; Chen, K. C.; Chang, H. T. *Electrophoresis* **2002**, *23* (15), 2477−2484.
(11) Salimi-Moosavi, H.; Jiang, Y.; Lester, L.; MacKinnon, G.; Harrison, D.; *Electrophoresis* **2002**, *21* (7), 1291−1299.
(12) Ingle, J. D., Jr.; Crouch, S. R. *Spectrochemical Analysis*; Prentice Hall: Englwood Cliffs, NJ, 1998.
(13) O'Keefe, A.; Deacon, D. A. G. *Rev. Sci. Instrum.* **1988**, *59*, 2544−2551.
(14) O'Keefe, A.; Scherer, J. J.; Cooksy, A. L.; Sheeks, R.; Heath, J.; Saykally, R. J. *Chem. Phys. Lett.* **1990**, *172*, 215−218.
(15) Vallance, C. *New J. Chem.* **2005**, *29*, 867−874.
(16) Paldus, B. A.; Kachanov, A. A. *Can. J. Phys.* **2005**, 83**,** 975−999.
(17) Berden, G.; Peeters, R.; Meijer, G. *Int. Rev. Phys. Chem.* **2000**, *19* (4), 565−607.

10.1021/ac060289o CCC: $33.50
Published on Web 07/20/2006

intensity in a high-finesse optical cavity, one can obtain a very sensitive measure for optical loss. From an exponential fit to the envelope of the intensity that is emitted for the cavity, one can determine the characteristic exponential decay time (ring-down time, RDT). This RDT depends only on the optical loss processes inside the cavity, but ideally not on the intensity of the incoming laser light pulse. Most importantly, in a cavity filled with an absorbing medium, the RDT is reduced, while the sensitivity and detection limit of the absorption measurement is enhanced by the increased effective absorption path length, which is frequently in the tens of kilometers. Conveniently, the sensitivity of the RDT measurement is largest when the optical absorption approaches zero.[18,19]

The application of CRDS to absorption measurements of condensed phases is more recent (van der Sneppen, L.; Wiskerke, A.; Ariese, F.; Gooijer, C.; Ubachs, W. W. *Anal. Chim. Acta* **2006**, *558*, 2.) and a number of technical approaches have been used in the past decade. Recent developments include the following: depositing a thin film onto the mirror surfaces,[20,21] situating a thin film in the cavity perpendicular to the lasers,[22,23] at Brewster's angle,[24,25] using a monolithic crystal,[26−29] or the use of a long optical waveguide loop[30] as a cavity to probe the absorption by the evanescent wave. Many of these techniques have been the subject of a recent review.[15]

In 2001, we developed a "mirrorless" condensed-phase absorption technique, which is similar to CRDS. In fiber-loop ring-down spectroscopy (FLRDS),[31−33] a loop made of optical waveguide material is used to confine the light instead of a ring-down "cavity" made with mirrors. Nanosecond laser pulses are injected into the fiber and are trapped in the waveguide for typically over 100 round trips. With each roundtrip, the laser pulse passes through the sample, which is situated between the ends of the optical fiber waveguide. The fractional loss in laser intensity is detected by a fast photodetector, and the ring-down time of the loop can be described by a single-exponential decay.

$$\tau = \frac{nL}{c_0(-\ln(T) + \alpha L + \sum_i \epsilon_i C_i d)} \quad (1)$$

Here ϵ_i is the extinction coefficient of an absorbing species i, C_i its concentration, and d the width of the absorption cell formed by the two fiber ends. The absorption losses of the fiber material are characterized by the length of the fiber loop, L, and the absorption coefficient of the fiber material, α. Finally the speed of light in the fiber is determined by the refractive index of the fiber core, n, and T is the transmission of the fiber−fiber joint in the absence of any absorber.

Recently, a refined technique, phase-shift FLRDS, was demonstrated to give a faster time response and enhanced sensitivity in the detection of a small amount of liquid sample.[34] In PS-FLRDS, an intensity-modulated continuous wave (cw) laser illuminates the fiber loop. The phase difference between the light entering the loop and exiting the loop is related to the ring-down time by $\tan(\Delta\phi) = -\tau\Omega$.[35] As a result, the magnitude of the phase shift can be used to perform quantitative concentration measurements.

In this paper, we present a simple approach to couple PS-FLRDS to CE for the online detection of labeled human serum albumin (HSA) samples. By further introducing a microlens, to reduce alignment losses across the sample gap, we improve both sensitivity and the limit of detection (LOD) compared to the square-cut fiber system. Samples were introduced into a capillary and detected either as static plugs or driven through the detection cell using pressure and electroosmotic flow. The performance parameters of the on-line FLRDS detectors are explored, such as the repeatability and the dynamic range. The lensed fiber detection system was applied to the analysis of HSA using a noncovalent label (cyanine dye, ADS805WS). The excess dye and the protein−dye complex were separated by CE. Performance parameters such as labeling ratio, repeatability, and dynamic range for the HSA analysis were also determined.

EXPERIMENTAL SECTION

Chemical Reagents. 2-[2-[2-Chloro-3-[(1,3-dihydro-3,3-dimethyl-1-(4-sulfobutyl)-2*H*-indol-2-ylidene)ethylidene]-1-cyclopenten-1-yl]ethenyl]-3,3-dimethyl-1-(4-sulfobutyl)-3*H*-indolium, inner salt, monosodium salt (ADS805WS) was purchased from American Dye Source, Inc. (Baie D.Urfe, PQ, Canada). HSA (>96%), sodium hydroxide, and boric acid were purchased from Sigma-Aldrich, Inc. (St. Louis, MO). These chemicals were used directly without any further purification, and all solutions were filtered by a 0.22-μm Millex-GV syringe filter unit (Millipore Corp., Bedford, MA). LePage 5-min epoxy glue was purchased from Henkel Canada Corp. (Brampton, ON, Canada). Deionized water (R > 18.2 MΩ) was prepared using a purification system with reverse osmosis treated feedstock.

Phase-Shift Fiber-Loop Ring-Down Spectroscopy System. An 80-m-long multimode optical fiber (AS100/140 IRPI, Fibertech Optica Inc.) was used to make a fiber loop (Figure 1).

(18) Jakubinek, M.; Tong, Z.; Manzhos, S.; Loock, H.-P. *Can. J. Chem.* **2004**, *82* (6), 873−879.
(19) Wheeler, M. D.; Newman, S. M.; Orr-Ewing, A. J.; Ashfold, M. N. R, *J. Chem. Soc., Faraday Trans.* **1998**, *94* (3), 337
(20) Curran, R. M.; Crook, T. M.; Zook, J. D. *Mater. Res. Soc. Symp. Proc.* **1988**, *105*, 175−180.
(21) Kleine, D.; Lauterbach, J.; Kleinermanns, K.; Hering, P. *Appl. Phys. B* **2001**, *72*, 249−252.
(22) Engeln, R.; Helden, G. v.; Roij, A. J. A. v.; Meijer, G. *J. Chem. Phys.* **1999**, *110*, 2732−2733.
(23) Logunov, S. L. *Appl. Opt.* **2001**, *40*, 1570−1573.
(24) Paldus, B. A.; Harb, C.; Zare, R. N.; Meijer, G. U.S. patent US6452680.
(25) Muir, R. N.; Alexander, A. J. *Phys. Chem. Chem. Phys.* **2003**, *5*, 1279−1283.
(26) Pipino, A. C. R.; Hudgens, J. W.; Huie, R. E. *Rev. Sci. Instrum.* **1997**, *68*, 2978−2989.
(27) Pipino, A. C. R.; Hudgens, J. W.; Huie, R. E. *Chem. Phys. Lett.* **1997**, *280*, 104−112.
(28) Pipino, A. C. R. *Phys. Rev. Lett.* **1999**, *83*, 3093−3096.
(29) Pipino, A. C. R. *Appl. Opt.* **2000**, *39*, 1449−1453.
(30) Tarsa, P. B.; Rabinowitz, P.; Lehmann, K. K. *Chem. Phys. Lett.* **2004**, *383* (3, 4), 297−303.
(31) Loock, H.-P.; Tong, Z.; Wright, A.; Jakubinek, M. 225th ACS National Meeting, New Orleans, LA, March 23−27, 2003.
(32) Brown, R. S.; Kozin, I.; Tong, Z.; Oleschuk, R. D.; Loock, H.-P. *J. Chem. Phys.* **2002**, *117* (23), 10444−10447.
(33) Tong, Z.; Jakubinek, M.; Wright, A.; Gillies, A.; Loock, H.-P. *Rev. Sci. Instrum.* **2003**, *74* (11), 4818−4826.
(34) Tong, Z.; Wright, A.; McCormcik, T.; Li, R. K.; Oleschuk, R. D.; Loock, H.-P. *Anal. Chem.* **2004**, *22*, 6594−6599.
(35) Engeln, R.; vonHelden, G.; Berden, G.; Meijer, G. *Chem. Phys. Lett.* **1996**, *262*, 105−109.

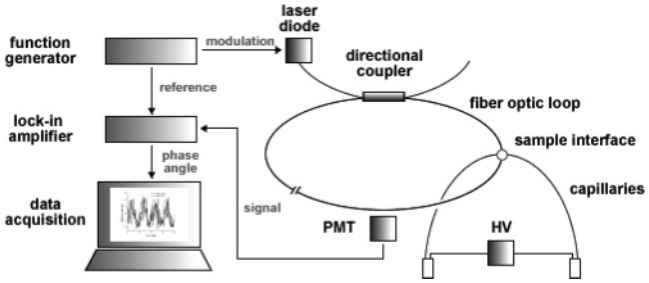

Figure 1. CE coupled with PS-FLRDS using a capillary/fiber interface. For pressure-induced flow measurements, the liquid was pumped through the capillary using a 6-port injector and a syringe pump, instead of the electrokinetically driven flow displayed here.

The two fiber ends were aligned on an $x-y-z$ translation stage in preliminary experiments and later in the capillary fiber interface. Using a microscope, the distance between the fiber ends could be easily determined and adjusted.

The output of an intensity-modulated cw diode laser (JDS Uniphase SDL-2372-P1, 810 ± 3 nm, maximum 2 W) was coupled into the loop. Two sine waves with identical frequency (100 kHz) and phase were produced using a function generator (LeCroy 9100 Arbitrary Function Generator). One was used as the reference for the lock-in amplifier, while the other one was applied as current modulation of the laser diode. The modulation current of the input is kept above the threshold of the emission and below the permissible maximum current to reduce signal distortion. A 2 × 2 optical fiber coupler (Lightel Technologies Inc., Kent, WA) with a splitting ratio of 1:99 was fused into the 80-m fiber loop (see Figure 1) to allow for coupling of the laser light into the loop. The loss associated with the two fusion splices (0.09 dB = 2.2%) was estimated from previous measurements,[33] while the splice quality determination provided by the fiber fusion splicer (Furukawa Electric Co. Ltd.) served as a rough guide. The insertion loss of the 2 × 2 coupler was not specified by the manufacturer, but is likely near 2−4% per pass (0.1−0.2 dB). A photomultiplier tube (PMT; Hamamatsu 950) is placed against the fiber loop a few meters away from the 2 × 2 coupler and monitors the light scattered from the fiber. The PMT signal is then fed into a fast lock-in amplifier (Stanford Research Systems SR 844) and referenced to the driving current of the laser diode. To reduce electromagnetic interference, all cables are shielded.

The phase shift, ϕ, can be recorded by comparing the phase angle of the light scattered from the fiber loop with that of the reference laser modulation. The data acquisition rate was set to 3.33 Hz, which provided a sufficiently high sampling frequency for electrophoretic and chromatographic measurements and permitted time integration over ~60 000 cycles. Due to inherent time delays in signal acquisition and processing, an offset phase angle, ϕ_0, has to be subtracted from the measured phase angle. As shown below, $-1/\tan(\phi - \phi_0)$ is linearly proportional to the concentration and therefore can be used directly to obtain an electropherogram. The data were then smoothed by a five-point average and the resulting peaks integrated using Microcal Origin software.

Lens Fiber Fabrication and Sensitivity Test. A microlens was made on one of the two fiber ends by controlled melting of the fiber end in the electric arc of a commercial fusion splicer. A hemispherical microlens with a radius of ~76 μm (shown in Figure 2) was readily fabricated and was shown to focus light into the core of the receiving fiber end.[36]

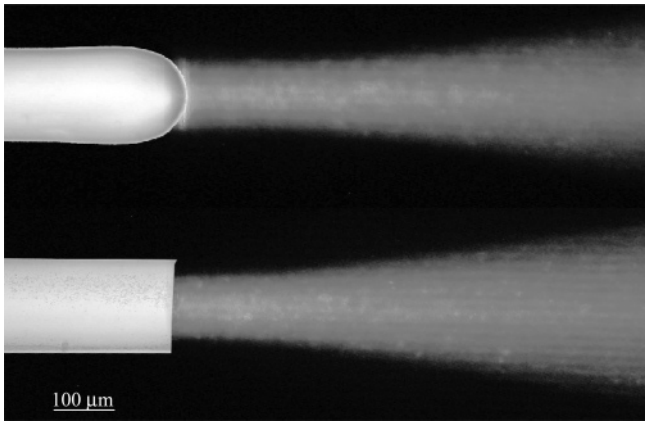

Figure 2. Composite photograph of the lensed fiber and straight fiber. The beam emitted from the fiber (λ = 632 nm) is photographed by suspending the fiber ends in a dilute milk emulsion. The core diameter of the fiber is 100 μm (cladding diameter, 140 μm).

To test the influence of the microlens on the sensitivity of detection, the lensed fiber and a receiving square-cut fiber were aligned using a translation stage (ThorLab Inc., Newton, NJ) under a 200× DigitalBlue QX3 microscope (Prime Entertainment Inc.). Nine different aqueous solutions with concentrations of AWS805DS dye up to 3.0 mM were suspended in the detection gap between the fiber ends, and the phase angle was recorded as a function of the concentration. For comparison, square-cut fibers were also tested by the same method. In both cases, the width of the detection gap was set to ~130 μm, positioned with the translation stage.

Fabrication of Capillary/Fiber Interface. To create the fiber-loop/capillary interface, a 150-μm channel was mechanically drilled through the center of the fused-silica capillary (i.d. 100 μm/o.d. 360 μm, Polymicro Technologies, Phoenix, AZ.). The drill bits (150-μm diameter, submicrograin tungsten carbide) were purchased from Drill Technology (Ada, MI). The drilling procedure is shown in Figure 3. First, the capillary was embedded in PMMA polymer by drilling a 360-μm-diameter hole into a block of PMMA and followed by insertion of the capillary into the hole. The capillary was then fixed using epoxy glue. Then, with the aid of a microscope, a 150-μm hole was drilled perpendicular to the long axis of the capillary through the PMMA and through the capillary. During the drilling process, a syringe pump (Harvard Apparatus, Holliston, MA) was used to pump water through the capillary (50 μL/min) to prevent the channel from clogging with glass particles (see Figure 3). The two ends of the fiber loop were then inserted into the precision-drilled hole and aligned to let the fiber ends meet with the inner capillary wall (~30 μm apart). Since the hole was drilled completely through the capillary, the fibers were easily aligned. The fibers were then sealed in place with epoxy glue. Since the drilled hole to facilitate the 150-μm fiber coupling is larger than the capillary inner diameter, we compensated for the additional volume by adjusting the fiber distance to 30 μm. The 10-μm gap remaining between the fiber and hole walls was filled with epoxy glue to ensure that no sample flow into this gap occurred.

(36) Loock, H.-P. *Trends Anal. Chem.* In press.

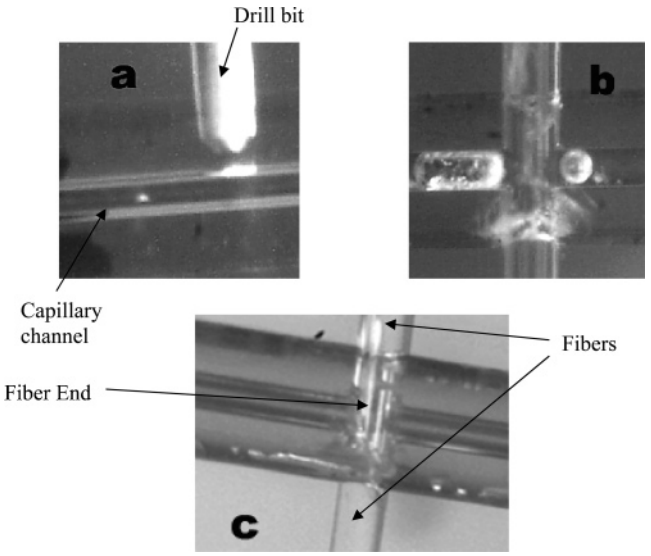

Figure 3. Drilling through a capillary and alignment of fiber ends. The capillary was first encapsulated in PMMA polymer block. (a) Drilling through the capillary. The drill bit (150-μm diameter) can be seen just above the channel (100 μm) of the 360-μm-o.d. capillary; (b) the channel drilled completely through; (c) fiber ends introduced into the channel (lens fiber on the top and square-cut receiving fiber on the bottom). The fibers were then sealed with epoxy glue.

Laser drilling into the glass capillary may be a viable alternative to mechanical drilling, but is in this particular case complicated. First the hole needs to be comparably deep (>350 μm) and small (150 μm) with minimal taper and precise dimensions. An additional problem is posed by the hollow core of the capillary, which is easily filled with debris. When using a mechanical drill, one can apply high pressure to the capillary core, but this is not an option when laser drilling.

Flow Injections and CE Separation Conditions. To test the phase angle response to different concentrations of ADS805WS, a series of dye solutions was introduced into the capillary/fiber interface by flow injection. A six-port injector with a 2-μL inner sample loop and a syringe pump (Harvard Apparatus) were used to inject sample solutions and drive a flow of 10 μL/min.

All capillary electrophoresis experiments were performed at room temperature (25 °C). The CE run buffer was a 10 mM borate buffer (pH 10.0). All buffers and samples were filtered and sonicated before use. The total length of the capillary was 60 cm, and the effective length for separation was 40 cm (i.e., from inject to detection window). The separation voltage was set to 30 kV (positive polarity mode) using a TriSep-2100 high-voltage module (Unimicro Technologies, Pleasanton, CA). Before the first use, the capillary was rinsed with 1 M sodium hydroxide for 30 min, followed by 20-min rinses with water and run buffer, respectively. After each run, the capillary was also rinsed with 1 M NaOH, water, and buffer for 3 min, respectively. Samples were introduced into the capillary by electrokinetic injection (5 kV for 10 s).

Noncovalent labeling of HSA with near-infrared (NIR) dye (ADS805WS) was performed by mixing the dye and protein solutions. The mixture was equilibrated by vortexing for 3 min (Vortex Genie 2, Scientific Industries, Inc., Bohemia, NY). The performance of the dye ADS805WS as a noncovalent label for serum albumin was investigated by testing various dye−protein ratios, while the total concentration of the dye was fixed at 1.5 mM.

RESULTS AND DISCUSSION

Fitting of the Concentration Dependence of the Phase Angle. As described by Engeln et al.,[35] the phase-shift, ϕ, and ring-down time, τ, are related simply by

$$\phi - \phi_0 = -\arctan(\Omega\tau) \tag{2}$$

where Ω is the intensity modulation frequency of the cw laser. The offset angle ϕ_0 contains all contributions due to the inevitable delays in the signal transmission and processing. It is constant for a particular experimental configuration but difficult to adjust or predict. In our analysis, the angle ϕ_0 is treated as a fitting parameter. Equation 2 illustrates that the ring-down time is proportional to $-\tan(\phi - \phi_0)$. Considering that $1/\tau$ is linearly dependent on the concentration of analyte between the two fiber ends of the fiber loop [or $1/(\tau - \tau_0)$ if the sample does not cover the entire cross section of the fiber core], a linear relationship also exists between $-1/\tan(\phi - \phi_0)$ and concentration. An electrophoregram/chromatogram is simply constructed by plotting $-1/\tan(\phi - \phi_0)$ versus time. The modulation frequency was set to Ω = 100 kHz; i.e., it was chosen such that $2\pi\Omega\tau \approx 1$ and the dynamic range of the phase angle measurement is maximized[35]

To determine ϕ_0 for each of the interfaces, eqs 1 and 2 can be combined[33]

$$\phi = \phi_0 - \arctan\frac{n\Omega L}{c_0(A + \epsilon dC)} \tag{3}$$

where $A = -\ln(T) + \alpha L$ is a constant related to the FLRDS system and depends on the absorption coefficient of the fiber material, α = 3.4 dB/km, and the transmission of the fiber−fiber splice, T, into which the sample is inserted. Values of ϕ_0 were determined by fitting of the concentration dependence of the phase angles, which were obtained, for example, by filling the capillary channel with sample solutions. The offset phase angle was determined to be −26.9° for the lens fiber/capillary fiber interface system. The effective width of the absorption path, d, was determined to be 25 μm. (see Figure 4), which compares well with the value of 30 μm obtained from the microscope image.

Influences of Lensed Fiber on the Detection Sensitivity. The sensitivity of the measurements and the detection limits critically depend on the background optical loss, i.e., the ring-down times (or phase angles) in the absence of any analyte. Ring-down spectroscopy is inherently more sensitive for very high finesse cavities. Since the optical waveguide material has an excellent transmission of 3.4 dB/km at 810 nm, most optical losses occur due to insertion loss of the fiber/fiber couplers and the coupling loss across the interface with the capillary. We have demonstrated that the coupling losses due to the effective numerical aperture of the emitting fiber end (NA = 0.07) for a multimode fiber are considerable, especially for gap widths exceeding 100 μm.[33] A microlens will reduce these losses by collimating or even focusing the multimode emitted light beam—compared to a square-cut fiber. In Figure 4, the lensed fiber

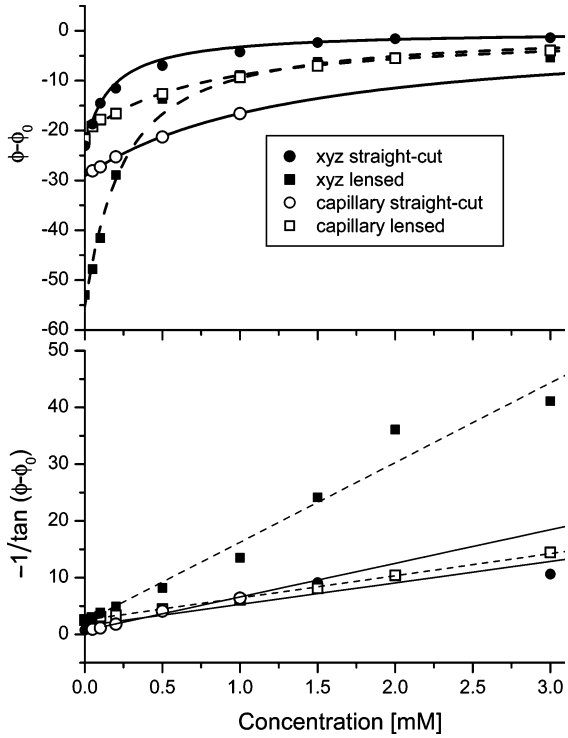

Figure 4. Change of the phase angle with respect to a reference phase angle, ϕ_0, as a function of dye concentration. The solid symbols show the measurements taken by aligning the fiber ends using a translation state. The curves are fits using eq 3 where A, d, and ϕ_0 were fitting parameters (see Table 1). The lower panel displays the same data but using $-1/\tan(\phi - \phi_0)$ as the observable, thereby indicating the good linear relation between the reciprocal phase angle and the concentration.

system shows an enhanced range of phase angles with improved optical coupling and consequently increased sensitivity and lower limits of detection. Here the lensed fiber end (solid squares) shows superior performance with respect to detection limit and sensitivity compared to the straight-cut fiber ends (solid circles). The open symbols show phase angle changes observed when the lensed fiber end was introduced into a capillary and the dye solutions were used to fill the entire capillary. Again, the lensed fiber (squares) shows a slightly improved sensitivity and LOD over the straight-cut fiber ends (circles). Typical for ring-down measurements, the sensitivity is largest for small concentrations as indicated by the slope at the intercept in Figure 4 (~80% greater for the lensed fiber; see Table 1). After accounting for the loss in the fiber material, the background loss is calculated from parameter $A = -\ln(T) + \alpha L$ (see eq 3) and is 15 and 40% per pass for the lensed fiber and straight-cut fiber ends, respectively. A large fraction of the background loss is due to the insertion loss of the commercial fiber−fiber couplers (up 4% per coupler per pass) as well as the fusion splices (2% per pass). Further improvements may be possible by replacing the couplers with evanescent couplers, by customizing the lens curvature, and by polishing both fiber ends to reduce scattering.

Capillary/Fiber Interface. The performance parameters of the interface of the capillary with the fiber loop containing a microlens were determined by using a series of aqueous solutions of ADS805WS dye. Typical flow traces and a peak area calibration curve of the capillary lens−fiber PS-FLRDS system are shown in Figure 5. Good repeatability was obtained for both peak area and peak height. The average relative standard deviation of the peak areas and peak heights were 3.65 and 3.97%, respectively. In the concentration range of 10 μM−2.0 mM, the peak areas show a linear response to the concentrations of ADS805WS ($R^2 = 0.99$); however, the linear response was lost at the concentration of 3.0 mM. The LOD was improved to 10 μM (α_{min}= 1.6 cm^{-1}), compared to the value obtained using the square-cut PS-FLRDS system (50 μM) (α_{min}= 8.0 cm^{-1}) in the capillary/fiber interface. Note, that the sensitivity and the LOD are improved for the lensed fiber system despite the fact that the transmission through the (larger) fiber/capillary interface is actually slightly smaller. The better transmission for the straight fiber interface arises from the much smaller width of the gap. While a small gap increases the transmission per pass, it does not influence the LOD or the sensitivity.

Table 1. Calibration Parameters for Three Different Fiber-Fiber Connections

	straight cut		lensed fiber	
	xyz stage	capillary/ fiber interface	*xyz* stage	capillary/ fiber interface
$A = -\ln T_{splice} + \alpha L$	0.58	0.44	0.17	0.64
T_{splice}[a]	0.60	0.65	0.85	0.56
ϕ_0 (deg)	−25.4	−74.7	−21.8	−26.9
d (μm)	86.1	10.4	35.4	25
sensitivity at "C = 0 mM" (deg/cm^{-1})	0.71	0.13	1.28	0.17
theoretical detection limit[b] $\alpha_{min} = \epsilon C$ (cm^{-1})	0.07	0.38	0.04	0.29
experimental detection limit[c] $\alpha_{min} = \epsilon C$ (cm^{-1})		8.0		1.6

[a] Calculated using $\alpha = 1.5 \times 10^{-4}$/m (corresponding to 3.4 dB/km). [b] Assuming 0.05deg can be measured. [c] Determined using S/N = 3.

Protein (HSA) Analysis by Noncovalent Labeling. (1) Optimization of CE Separation Conditions. The capillary electrophoretic conditions, such as buffer concentrations and pH values, were optimized so that the free dye and the dye−protein complex could be resolved. The pH value of a run buffer is a very important factor for CE separations. Due to the protein absorption on the wall of capillary during the CE separation processes, a run buffer with pH values greater than the isoelectric point (pI) of the protein should be used to minimize the absorption. In the present work, three pH values of 8.0−10.0, which are much greater than the pI value of HSA, were examined, and it was found that of these a run buffer with pH 10.0 provided the best resolution (see Figure 6). The optimum ionic strength (10 mM) was determined by varying the boric acid concentration from 10 to 200 mM.

(2) HSA Analysis by Noncovalent Labeling. HSA, the most abundant serum protein, may best be known for its ability to reversibly bind a variety of drugs with different physical and chemical properties.[37] The binding of a drug to HSA influences the drug's toxicity, activity, solubility, distribution, and excretion.[37] As a result, a drug's efficacy can be significantly affected by drug−

(37) Peters, T. *All about albumin: biochemistry, genetics, and medical applications*; Academic Press: San Diego, CA, 1996; pp 76−131.

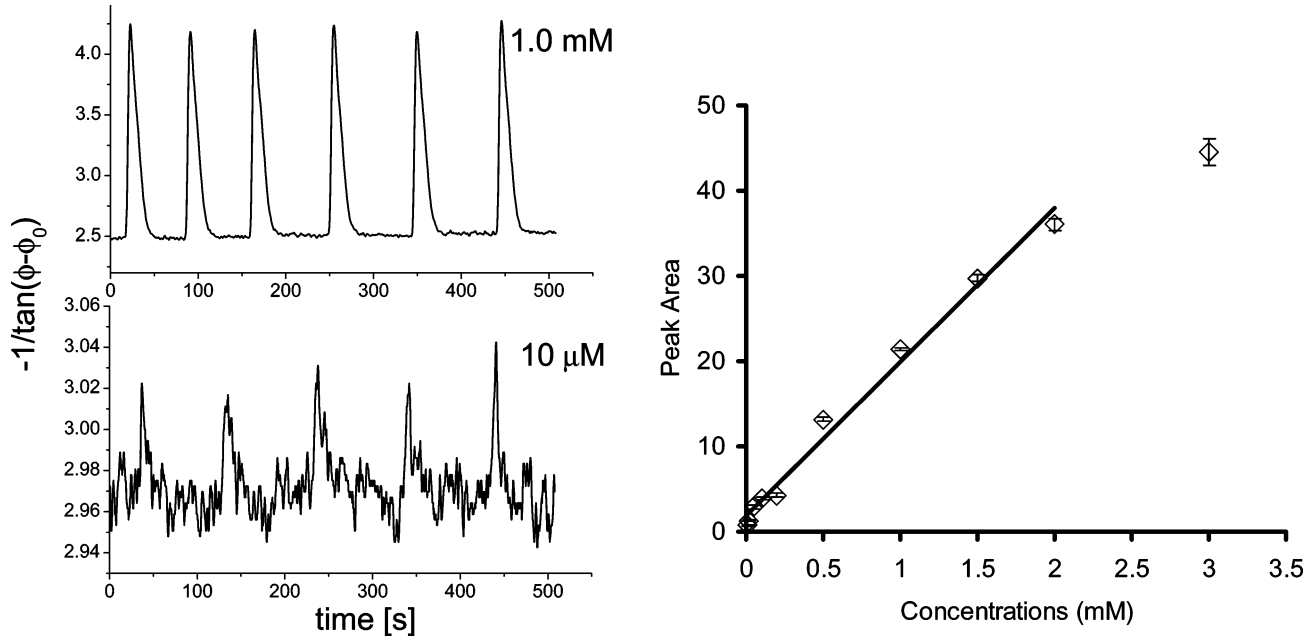

Figure 5. Flow traces for two concentrations of ADS805WS (1.0 mM and 10 μM) probed by PS-FLRDS at 810 nm in the homemade capillary fiber interface using the lensed emitting fiber. In both cases, the injection volume was 2 μL, flow rate was 10 μL/min, and acquisition rate was 3.33 Hz. The average RSD of peak areas and peak heights are 3.65 and 3.97%, respectively. The calibration curve for this configuration was obtained by averaging the peak areas for each injection and is shown on the right.

albumin interactions. Therefore, it is necessary to develop methods to determine the amount of HSA, rapidly.[38]

It has long been known that dyes have the ability to reversibly bind to serum albumin.[37] Fluorescent dyes are ideal probes to study albumin due to low background signal compared absorption measurements and the consequent improved sensitivity.[1] However, autofluorescence from the sample matrix is a source of interference, which is encountered when using visible dyes. The use of NIR dyes practically eliminates background fluorescence since very few molecules possess intrinsic fluorescence in the NIR region (λ: 670−1000 nm). Consequently, NIR dyes are well-suited for bioanalytical applications, where sample matrix autofluorescence is a potential source of interference.[39−46] NIR dyes have good photophysical properties, with molar adsorptivities of 150 000−250 000 L mol^{-1} cm^{-1}.

In the present work, a cyanine dye, ADS805WS, was used to noncovalently label HSA. The advantages of noncovalent labeling schemes are that they are fast, pH control is not necessary, and purification procedures may not be needed.[38,47] The electropherograms in Figure 7 illustrate the effect of increasing HSA concentrations in the solutions with a fixed total dye concentration of 1.5 mM. The first 60 s of the electropherogram are related to the injection procedure, and the separation is obtained in ~2 min. When the concentration of protein is large, the peak resulting from the dye−protein complex increases while the free dye peak

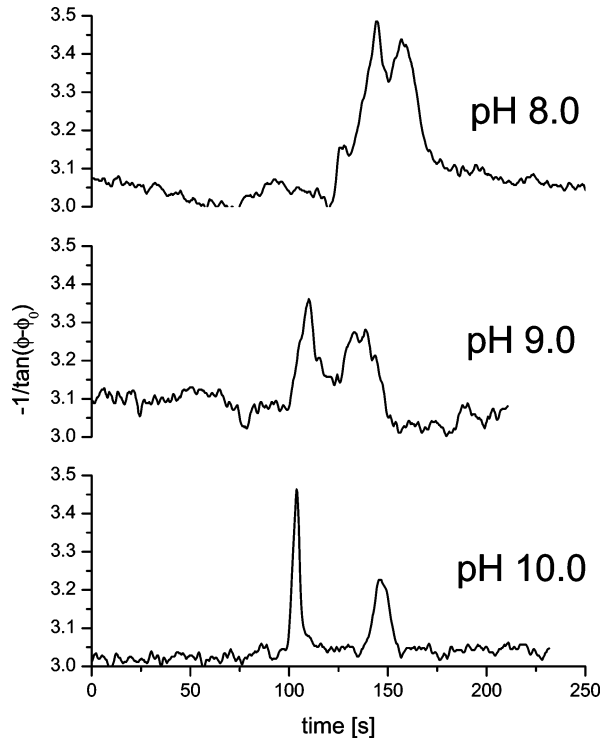

Figure 6. Electropherograms of dye and protein mixture using run buffers with different pH values. The first peak is related to free dye, and the second peak is related relative to the dye−protein complex. The run buffer is 10 mM boric acid, and the separation voltage was set at 30 kV. Sample solutions were electrokinetically injected using 5 kV for 10 s.

(38) Sowell, J.; Mason, J. C.; Strekowski, L.; Patonay, G. *Electrophoresis* **2001**, *22*, 2512−2517.
(39) Baas, M. J.; Patonay, G. *Anal. Chem.* **1999**, *71*, 667−671.
(40) Sheally, D. B.; Lipowska, M.; Lipowski, J.; Narayanan, N.; Sutter, S.; Strekowski, L.; Patonay, G. *Anal. Chem.* **1995**, *67*, 247−251.
(41) Soper, S. A.; Mattingly, Q. L.; Vegunta, P. *Anal. Chem.* **1993**, *65*, 740−747.
(42) Lee, Y. H.; Maus, R. G.; Smith, B. W.; Winefordner, J. D. *Anal. Chem.* **1994**, *66*, 4142−4149.
(43) Williams, D. C.; Soper, S. A. *Anal. Chem.* **1995**, *67*, 3427−3432.
(44) Legendre, B. L., Jr.; Moberg, D. L.; Williams, D. C.; Soper, S. A. *J. Chromatogr., A* **1997**, *779*, 185−194.
(45) Flanagan, J. H., Jr.; Owens, C. V.; Romero, S. E.; Waddell, E.; Kahn, S. H.; Hammer, R. P.; Soper, S. A. *Anal. Chem.* **1998**, *70*, 2676−2684.
(46) McWhorter, S.; Soper, S. A. *Electrophoresis* **2000**, *21*, 1267−1280.
(47) Moody, E. D.; Viskari, P. J.; Coyler, C. L. *J. Chromatogr., B* **1999**, *729*, 55−64.

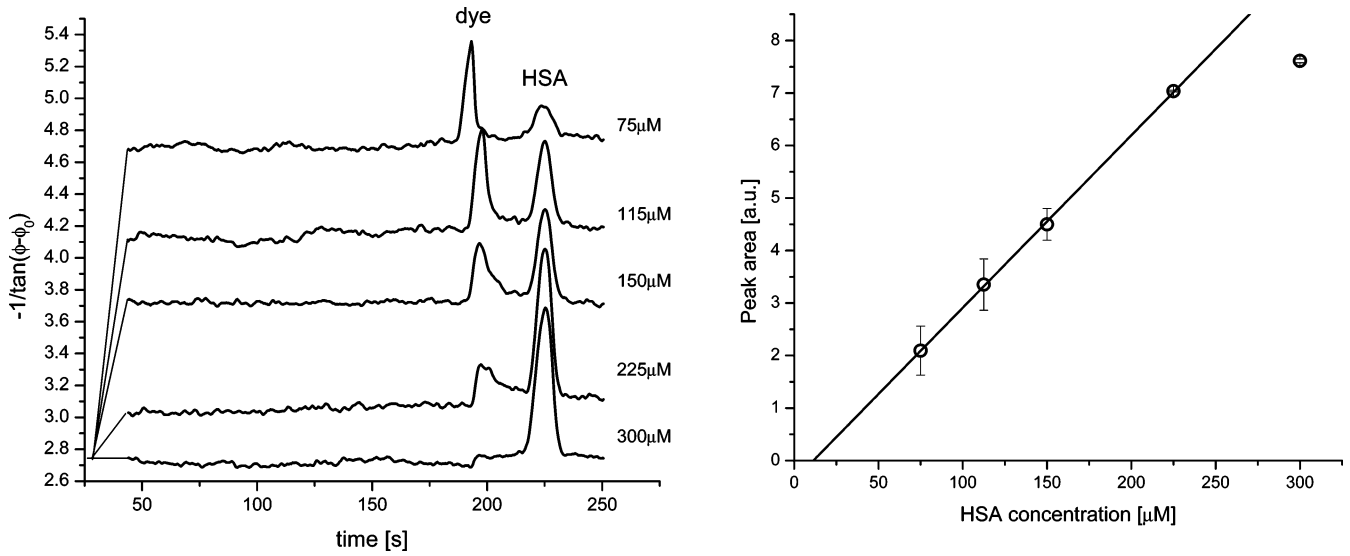

Figure 7. Electropherograms of samples with different protein concentrations (0.075−0.3 mM) and fixed dye concentration of 1.5 mM. CE conditions: 10 mM boric acid run buffer, pH 10.0; separation voltage, 30 kV. The samples were injected using 5 kV for 10 s. Curves are offset from the common phase angle for clarity. As shown on the right, there is a linear correlation between the peak areas of the labeled HSA in the electropherograms and the HSA concentration. The deviation at the highest concentration is indicative of incomplete labeling of the serum albumin.

decreases, which suggests that the cyanine dye of ADS805WS is a suitable label of HSA analysis. Assuming that the absorption coefficient of ADS805WS in the HSA environment is similar to the absorption coefficient of the free dye, one can determine the labeling coefficient between 5:1 to 7:1 (Table 2) by simply comparing the peak areas of the free dye and the dye−protein complex.

The linear response of the dye−protein complex peak areas to protein concentrations was examined by the using the electropherograms in Figure 7. Figure 7 shows an excellent linear response ($R^2 > 0.99$) in the concentration range of 75−225 μM. However, the linear response was lost for the highest protein concentration (300 μM HSA). Given the HSA/dye ratio of 1:5, the departure from linearity is likely due to the incomplete labeling of the protein. Reasonable repeatability was obtained with the average RSD of peak areas of 8.68% (4 parallel runs).

From the ~1:6 labeling ratio and considering that the detection limit for the ADS805WS dye has been determined to be 10 μM (flow injection data, above), the detection limit of labeled HSA can be estimated as 1.67 μM. Using the detection limit of the static plug (LOD = 1.8 μM), and assuming that a phase angle shift of 0.05° is measurable at the instrumental limit, a theoretical detection limit of 300 nM dye-labeled HSA is achievable (see Table 1).

It is more difficult to assess the fundamental detection limit of this technique. Time-resolved cavity ring-down measurements are limited in their sensitivity by a combination of fractional absorption loss, cavity length, and absorption path length.[18] The shot noise limit may be encountered when sampling at very high rates and low intensity levels. By contrast, phase-shift detection is inherently relying on averaging of a comparably intense modulated signal—typically at data acquisition rates slower than 100 Hz. It is not likely that shot noise limitations will be encountered. The detection of noncovalent labeled HSA is meant to be illustrative of the ability to use phase-shift ring-down measurements for absorption detection. Currently, other fluorescent labeling strategies for protein determination are significantly[48] more sensitive (typically picomolar detection limits) than the current ring-down instrumentation.

Table 2. Labeling Coefficient of HSA and the Dye of ADS805WS

concentration (μM)	300	225	150	115	75
ratio (HSA/dye)	1/5	1/6.7	1/10	1/13.3	1/20
labeling factor	*a*	4.8	5.7	6.0	7.0

[a] Not obtained because the free dye peak was too small for analysis.

CONCLUSION

A simple method was developed to fabricate a microlens on the end of a fiber, which can focus light into the receiving fiber, so that the losses related to the fiber-loop cavity are lowered. By using the lensed fiber in phase-shift fiber-loop ring-down spectroscopy, the detection sensitivity was improved by up to 80%. Furthermore, the PS-FLRDS detector was coupled to CE as an online detector by drilling a 150-μm hole through the center of the capillary channel perpendicular to its long axis. The performance parameters of the online detector were examined by introducing a series of sample solutions with different concentrations using flow injection. The detection limit could be determined to be 10 μM, which is 5 times smaller than that shown for a previous square-cut fiber system. This corresponds to the detection of 5.3 fmol of sample in a 530-pL volume.

To further characterize the abilities of the PS-FLRDS detection in a CE separation, we applied the system to the separation and analysis of HSA. The protein was noncovalently labeled by a NIR dye. The excessive free dye and the dye−protein complex were resolved using a run buffer of 10 mM boric acid with pH 10.0. The labeling coefficient was determined to be ~6. Furthermore,

(48) Rech, I.; Restelli, A.; Cova, S.; Ghioni, M.; Chiari, M.; Cretich, M, *Sens. Actuators, B* **2004**, *100*, 158−162.

an excellent linear response (R^2 > 0.99) was obtained when correlating the peak areas and concentration of HSA, resulting in a calculated detection limit of 300 nM.

PS-FLRDS provides a simple, inexpensive, and convenient method for interrogating samples in systems where only a minimal path length is available (e.g., in microfluidics) and is particularly well suited to analyze samples in the NIR region of the spectrum.

ACKNOWLEDGMENT

The authors thank Zhaoguo Tong, Dan Courtney, and Nicholas Trefiak for many useful discussions and technical assistance. We also acknowledge the Natural Sciences and Engineering Research Council of Canada, the Canadian Foundation for Innovation, the Canadian Initiative for Photonic Innovations, the Ontario Innovation Trust, Premier's Research Excellence Award, Photonics Research Ontario, and Queen's University for financial support.

Received for review February 15, 2006. Accepted June 2, 2006.

AC060289O